Simplified CFD for pressure drop predictions in ducts

Thijs van Druenen [a], *Zakarya* Kabbara [b], *Ivan* Verhaert [b], *Twan* van Hooff [a]

[a] Building Physics and Services, Department of the Built Environment, Eindhoven University of Technology, PO Box 513, 5600, MB Eindhoven, the Netherlands, t.v.druenen@tue.nl

[b] Energy and Materials in Infrastructure and Buildings (EMIB - HVAC), University of Antwerp, Campus Groenenborger (Building Z), Groenenborgerlaan 171, Antwerp 2020, Belgium

Abstract. In the design of a ventilation system, the ductwork is generally composed based on analytical equations in combination with loss coefficients. This widely used approach can lead to large deviations in the prediction of the total pressure drop. Poor performance optimization could on its turn lead to a higher energy demand. While the use of computational fluid dynamics (CFD) could improve this prediction, it is often not feasible in practice as the use of CFD requires a high computational demand and a high-level of expertise. An alternative could be the use of simplified CFD. In this study the application of several conventional and simplified CFD methods and analytical prediction methods in the ventilation system design process was assessed. The simplified CFD methods include the use of coarse-grid CFD and voxel-based CFD simulations. Measurements on a single and double elbow configuration were performed and were used for validation purposes. For the investigated configurations the analytical prediction started to deviate from the measurements with increasing complexity of the system. For the conventional and coarse-grid CFD methods the prediction of the pressure drop was highly sensitive to the applied near-wall treatment and roughness parameters. For the voxel-based CFD method an average percentage difference of only 3% with respect to the measurements was found for the single elbow configuration. However, it overestimated the measured pressure drop by 64% on average for the double elbow configuration. A general sufficiently accurate method for predicting the pressure drop, which would also be feasible for use in practice ventilation system design, was not yet found. As this paper is part of a larger study, the assessment of additional simplified CFD methods on more complex duct configurations is the subject of future work.

Keywords. Computational Fluid dynamics, Simplified CFD, Ventilation system design, Ducts.
DOI: https://doi.org/10.34641/clima.2022.304

1. Introduction

The design of the ductwork of a ventilation system is primarily based on analytical equations in combination with loss coefficients (e.g. [1,2]). While this is a widely used approach, it is well-known that this can lead to large deviations in the prediction of the total pressure drop [3-5]. Former research indicated that the application of computational fluid dynamics (CFD) simulations could reasonably predict the pressure drop in ventilation systems [6-10]. Shattered agreements were found in early numerical studies. Mumma et al. [6] conducted a numerical study on a configuration of coupled fittings, but found a large underprediction while comparing the calculated loss coefficient for the isolated fittings to the ASHRAE duct fitting database (DFDB). By application of steady RANS and the standard k-ε turbulence model the loss coefficient was underestimated by 28% for a 90° rectangular elbow fitting with a large radius and by 62% for a 90° elbow fitting with a small radius. In a later study, Mumma et al. [7] numerically calculated the loss coefficients for nine fittings. By application of the standard k-ε turbulence model the computed results were within ±15% of those found in the ASHRAE DFDB for seven of the nine fittings. Moujaes and Deshmukh [8] found pressure drop differences of 8% for an elbow fitting, and 8% and 18% for respectively the straight and branch flow in a tee fitting, while comparing their numerical results tot the ASHRAE DFDB. Liu et al. [9] performed CFD simulations and compared the results of three CFD approaches with experimental data from literature. The study found that the calculated pressure drop was very sensitive to the modeled surface roughness in the straight parts of the configuration. After determination of suitable roughness parameters the pressure drop could accurately be predicted by steady RANS methods using the standard k-ε turbulence model or Reynolds stress model. The LES method failed in accurately predicting the pressure drop. However, a relatively coarse grid in terms of LES requirements was used. Manning et al. [10] calculated the loss

coefficient for a flat-oval straight-body lateral and a flat-oval straight-body tee. Their CFD simulations compared well quantitatively against experimental results for the majority of the configurations and considered CFD a viable tool to accurately predict the correct loss coefficient curve-shaped structure as a function of flow rate.

This brief literature review indicated that the performance of CFD was diffuse, but it showed potential of being a valuable tool for predicting the pressure drop. However, application of CFD is not feasible in ventilation design practice as the application of conventional CFD requires large computational resources, long computation time and a high-level of expertise. An alternative could be the use of simplified CFD to lower computation time and limit the required knowledge for performing such simulations ([11-14]). The application of simplified CFD could improve the prediction of pressure drop during the early phases of the design process compared to the use of analytical methods, while limiting the computational demand compared to conventional CFD. Several options are present in literature, for example fast fluid dynamics (e.g. [11]), lattice Boltzmann (e.g. [12]), coarse grid CFD (e.g. [13]), CFD with zero-equation turbulence model (e.g. [14]). Each method has its potential strengths and weaknesses and therefore further analysis is needed.

In this study the application of several prediction methods in the ventilation system design process was assessed. Numerical (CFD) and analytical (ASHRAE) methods were applied to two duct configurations. The CFD methods included the use of high-quality CFD on high-resolution grids and simplified CFD by the use of CFD on low-resolution grids and the use of voxel-based CFD using ANSYS Discovery Live 2020r1 [15]. Measurements on both duct configurations were performed and were used for validation purposes. The purpose of the current project is to find a fast and user-friendly tool, with an improved accuracy over conventional analytical methods, which can be used by engineers without the need for extensive expert knowledge on CFD.

2. Measurements

The full-scale experimental models are shown in Fig. 1. The system was composed of a centrifugal fan, circular air ducts and, depending on the tested configuration, one or two 90° elbows. The system was supported by angle brackets at approximately 1 m height. The circular ducts and elbows had a radius of 100 mm. The elbow characteristics are shown in Fig, 2 with r/D = 1 and D = 200 mm. The components were manufactured of galvanized sheet steel, sealed and connected using steel duct clamps.

Two measurement configurations were tested:

A. Single 90° elbow configuration

B. Double 90° elbow configuration

The measurements were performed according to ASHRAE Standard 120-2017 [16]. This standard prescribes a minimum of eight test velocities, evenly distributed over the total range. The recorded mean flow velocities per configuration are given in Table 1. As the primary goal of this study is the validation of CFD methods, also less-common higher flow rates were investigated. The velocity was unevenly distributed in the duct section. Therefore, velocity measurements were performed at 18 points in the duct's cross sections according to the ASHRAE Handbook [18]. Measurements were performed by the Testo 0635 9542 digital vane probe together with the Testo 480 meter and 10 s average values were noted. The area-average streamwise velocity of this section was taken as the average of these 18 velocity measurements [18].

Tab. 1 - Mean inlet velocities in m/s

A. Single bend	B. Double bend
2.52	2.49
3.22	3.14
4.23	4.13
5.29	5.09
6.68	6.33
7.68	7.52
8.79	8.52
10.09	9.67

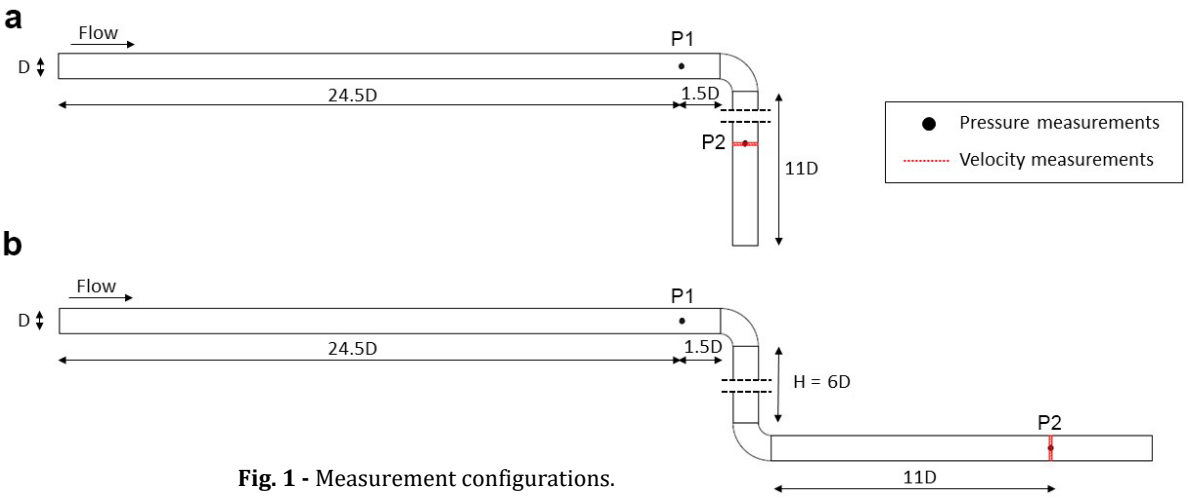

Fig. 1 - Measurement configurations.

A duct length of 4.9 m between the fan and first measurement point P1 was applied to ensure that the air flow was fully developed. A distance of 1.5D (300 mm) was used between P1 and the fitting and the length between the fitting and P2 was 11D (2200 mm). The pressure loss between these points was evaluated for eight flow rates per configuration.

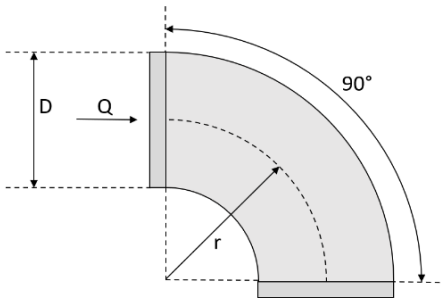

Fig. 2 - Elbow fitting with r/D = 1 and D = 200 mm.

In accordance with the ASHRAE Standard 120-2017 [16] the static pressure differential measurements were performed by simultaneously lowering two pitot-static tubes parallel to the flow in the duct at both P1 and P2. The pitot-static tubes were connected to a Testo 480 pressure transducer [17] and 10 s average values were noted. Measurements of temperature, atmospheric pressure and humidity were performed before each pressure measurement using the Testo 0632 1543 digital IAQ probe together with the Testo 480 meter. The measuring range and accuracy of the instruments is presented in Table 2.

Tab. 2 - Instrumentation details

Instrument	Range	Accuracy
Testo 480 meter	-100 – 100 hPa	±0.3 Pa + 1%
Testo 0635 9542 digital Vane probe	0.6 – 50 m/s	± 1%
Testo 0632 1543 digital IAQ probe	0 – 50 °C	± 0.5°C
Testo 0632 1543 digital IAQ probe	0 – 100% RH	±1.4%
Testo 0632 1543 digital IAQ probe	700 – 1100 hPa	± 3 Pa

The measured friction factor of the circular duct and the loss coefficient of the fitting, both required for the analytical prediction method (see Section 3) were calculated based on straight duct measurements performed in accordance with ASHRAE Standard 120-2017 [16]. Here, configuration A was used (Fig. 1) with exclusion of the elbow fitting. The measured friction factor f_{meas} was determined by:

$$f_{meas} = \frac{\Delta p_{f,1-2}}{p_v/D_h} \quad (1)$$

in which D_h is the hydraulic diameter (0.2 m), p_v the dynamic pressure and $\Delta p_{f,1\text{-}2}$ the total pressure loss per meter of straight duct and calculated using:

$$\Delta p_{f,1-2} = \frac{\Delta p_{s,1-2}}{L_{1-2}} \quad (2)$$

Here, $\Delta p_{s,1\text{-}2}$ is the measured pressure difference between P1 and P2 and $L_{1\text{-}2}$ the length between P1 and P2. The local loss coefficient C_{meas} of the fitting is determined using:

$$C_{meas} = \frac{\Delta p_{t,1-2}}{p_v} \quad (3)$$

In which $\Delta p_{t,1\text{-}2}$ is the measured pressure difference $\Delta p_{s,1\text{-}2}$ minus the share of the straight duct between P1 and P2 with length L_{SD}:

$$\Delta p_{t,1-2} = \Delta p_{s,1-2} - L_{SD} * \Delta p_{f,1-2} \quad (4)$$

3. Analytical prediction

In this study the analytical prediction of the pressure drop is based on the ASHRAE Handbook [19]. This prediction method distinguishes between friction losses, in straight parts, and dynamic losses due to fittings. For fluid flow in straight ducts the friction loss in terms of total pressure can be calculated by the Darcy equation:

$$\Delta p_{f,calc} = \frac{f L_{SD} p_v}{D_h} \quad (5)$$

Here f is the friction factor, which can be measured (see Equation 1) or calculated by the Colebrook equation:

$$\frac{1}{\sqrt{f_{calc}}} = -2log\left[\frac{\epsilon/D_h}{3.7} + \frac{2.51}{Re\sqrt{f_{calc}}}\right] \quad (6)$$

where ϵ the absolute pipe roughness and Re the Reynolds number of the flow. ASHRAE prescribes a pipe roughness ϵ = 0.09 mm for galvanized steel. Dynamic losses result from flow disturbances caused by duct mounted equipment and fittings that change the airflow's direction or cross-sectional area. For an elbow the total pressure loss over this fitting Δp_e can be calculated by:

$$\Delta p_e = C * P_v \quad (7)$$

Here, C is the loss coefficient for this particular fitting, which can be obtained by measurements (see Equation 3) or be found in manufacturer's datasheets or fitting databases (e.g. [20]). In this study the analytical prediction outlined above was performed for two sets of input conditions. In the first analytical prediction method (AP-I) the friction losses were determined based on f_{calc} (see equation 6) and the loss coefficient C_{ASHRAE} = 0.25 was obtained from a fitting database [20]. In AP-II the measured friction factor f_{meas} was used, which was calculated based on measurements on a straight duct part. The elbow loss coefficient was based on equation 3 in which C_{meas} was calculated from measurements for configuration A.

4. CFD simulations

In this study the performance of several simulation methods on the prediction of the pressure drop was assessed. The methods were classified with respect to theoretical accuracy and simulation time (this included time for pre/post processing). The three categories were named CFD-I, CFD-II and CFD-III, with CFD-I being the most, and CFD-III being the least theoretically accurate and time-consuming method. With respect to simulation time, one can think of CFD-I in the order of days to a week, CFD-II in the order of hours to days and CFD-III in the order of minutes to hours. The CFD-I simulations were characterised by solving the flow down to the viscous sublayer near the wall and is, in essence, required for an accurate prediction of separation and reattachment of the flow. This required a high-resolution grid in these areas. Two turbulence models were assessed, e.g. the realizable k-ε model (RLZ-I) [21] and the k-ω SST model (SST-I) [22]. In the CFD-II approach a simplified form of regular CFD is applied in which the flow was modeled in the near-wall region. This allowed the use of larger cells in these areas. The realizable k-ε model (CFD-II) [21] was used. The CFD-III method included a voxel-based simplified CFD approach using the ANSYS Discovery Live package (CFD-III) [15]. Based on GPU computing, this software allows almost instantaneous simulation results.

4.1 Computational domain

Figure 3a shows the computational domains for the CFD-I and CFD-II methods, for both configuration A and B. The computational domains were constructed with equal dimensions as the ductwork used in the measurements. The surface at the upstream side of the domain was modeled as velocity inlet and the surface at the downstream side of the domain was modeled as pressure outlet. The duct inner surfaces were modeled as no-slip walls and sampling planes P1 and P2 were created at locations similar to the measurements. Due to limitations of the software, only the section between P1 and P2 was modeled for the CFD-III method.

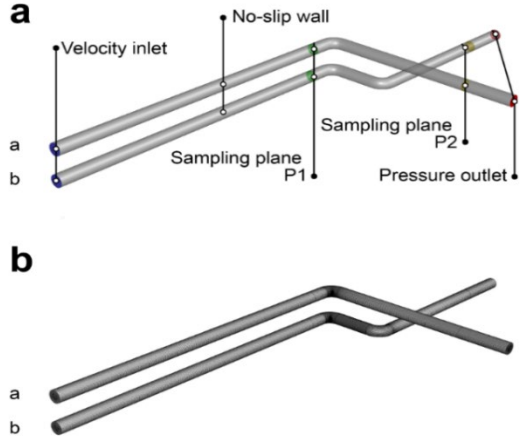

Fig. 3 - Computational (a) domains and (b) indicative grids for CFD-I and CFD-II.

4.2 Computational grid

Grid-sensitivity analyses were conducted for CFD-I and CFD-II methods using configuration A. It was assumed that the resulting grid topology for configuration A (single elbow) was sufficiently fine for configuration B (double elbow) as well. The grids were constructed using a sweep method [23]. Grid topologies are found in Table 3. The surface plane at the inlet of the computational domain was meshed according to the characteristics first cell height, growth rate, cell layers and cells over circumference, after which this meshed surface was swept with given cell lengths to create the 3D volume grid. To resolve the boundary layer at the surface in the CFD-I simulations, the normal distance of the cell center point from the wall surface y_P was determined so that y* is lower than 2.5 (coarse), 1.3 (medium), 0.6 (fine) and 0.3 (finest) for the highest inlet velocity (≈ 10 m/s). The dimensionless wall unit y* is defined by $y^*=u^*y_P/\nu$ where u* is the friction velocity and ν is the local kinematic viscosity. For the CFD-II simulations, y_P was determined so that y* is higher than 50 for the lowest inlet velocity (≈ 2.5 m/s).

CFD-I required the analysis of four systematically refined grids (see Fig. 4a-d), while for CFD-II the performance on three grids was assessed (see Fig. 4e-g). The results are presented in Section 5.1. The CFD-III simulations did not allow much control on the grid. It automatically constructs a uniform voxel-based grid for its user. By putting the fidelity function at its maximum value the grid was constructed with the highest resolution.

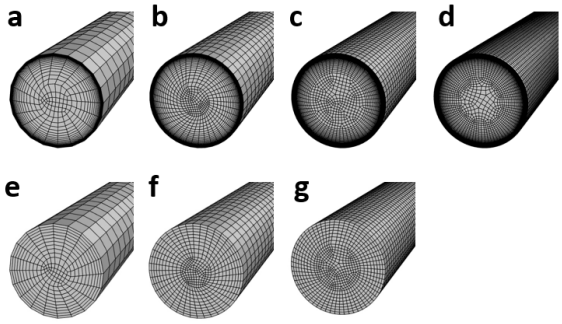

Fig. 4 – (a-d) CFD-I and (e-g) CFD-II grid topologies.

4.3 Computational settings

3D steady RANS simulations were performed in full scale. The CFD-I and CFD-II simulations were performed using the commercial CFD code ANSYS Fluent 21r1 [24], for which pressure-velocity coupling was performed by the SIMPLEC algorithm, gradients were computed with the least square cell based scheme, pressure interpolation was second order and second-order upwind discretization schemes were used for the convection and viscous terms of the governing equations. The simulations were considered converged as an increasing number of iterations did not lead to changes in the monitored pressure drop $\Delta p_{t,1\text{-}2}$.

Tab. 3 – Grid characteristics

Grid resolution		First cell height (mm)	Growth rate	Cell layers	Cells over circumference	Cell length (m)	Cell length in bend (m)
CFD-I a	Coarse	0.08	1.2	28	20	0.06	0.015
CFD-I b	Medium	0.04	1.15	40	40	0.04	0.010
CFD-I c	Fine	0.02	1.1	56	60	0.02	0.005
CFD-I d	Finest	0.01	1.1	60	80	0.01	0.003
CFD-II e	Coarse	5	1.07	10	20	0.06	0.015
CFD-II f	Medium	5	1.07	10	40	0.04	0.010
CFD-II g	Fine	5	1.07	8	60	0.02	0.005

For the CFD-III simulations ANSYS Discovery Live 2020r1 [15] was used. Internal fluid simulations were performed with the steady state fluids solver. This solver is based on a cell-centered Cartesian finite volume discretization according to Ye et al. [25]. Uniform discretization is applied, together with a voxelized level-set approach starting from the geometry. An iterative algorithm similar to the SIMPLE scheme is applied and turbulence is modeled using a standard k-ε model.

4.4 Boundary conditions

At the inlet of the domain a uniform mean velocity was imposed, equal to the magnitude of the mean flow velocity as recorded in the measurements (see Tab. 1). Turbulence was specified by a turbulent intensity of 5% and a turbulent viscosity ratio of 10. Their impact was evaluated to be negligible due to the large distance between the inlet of the domain and P1. Zero static gauge pressure was specified at the outlet. In case the method allowed, roughness was applied at the duct wall surfaces by definition of the equivalent sand-grain roughness height k_S. Fitting with straight duct measurement yielded k_S = 0.0005 m for SST-I and k_S = 0.0006 m for CFD-II.

5. Results

5.1 Grid-sensitivity analyses

The results of the grid-sensitivity analyses were evaluated in terms of percentage deviation in pressure drop $\Delta p_{t,1\text{-}2}$ with respect to that on the finest grid tested and are presented in Figure 5. The results for CFD-II were compared to the results found on the fine grid, while for the CFD-I methods the result were evaluated with respect to $\Delta p_{t,1\text{-}2}$ obtained on the finest grids. The results for CFD-II on both the coarse and medium grids showed differences of 0.2% with respect to the fine grid and therefore the medium grid was retained for the CFD-II method in the remainder of this study. Much larger differences were found for the CFD-I methods and therefore an additional fourth (finest) grid was required. For SST-I differences of 8.2% (coarse), 3.9% (medium) and 1% (fine) were found with respect to the finest grid. Percentage differences of 1.2%, 0.4% and 0.2% were obtained on respectively the coarse, medium and fine grid for RLZ-I. These agreements were considered as nearly grid-independent results and therefore the medium grid was retained for the CFD-I methods.

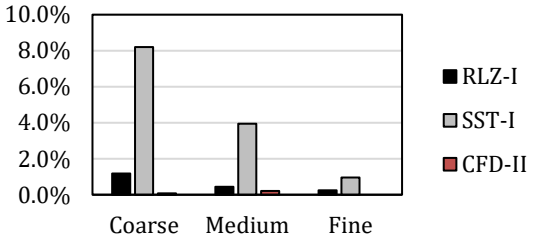

Fig. 5 - Grid-sensitivity analyses results in terms of percentage pressure drop $\Delta pt_{,1\text{-}2}$ with respect to that on the finest grid tested.

5.2 Configuration A: Single elbow

Figure 6 gives the results for all investigated methods for configuration A. The results are presented in terms of $\Delta p_{t,1\text{-}2}$ as function of Q. In agreement with literature, a quadratic relation was observed for all methods. Based on the measurement results, an average loss coefficient C_{meas} of 0.29 was calculated for the 90° elbow fitting using Equations 3 and 4. This loss coefficient C_{meas} was used for the calculation of AP-meas. As a result of this tuning process, the average agreement over all values for Q between AP-meas and the measurements was fair with an average absolute percentage difference *AAPD* of 7%. An AAPD of 13% was calculated for AP-calc. However, the best agreement with the measurements was observed for CFD-III with an AAPD of 3%. SST-I and CFD-II both showed an overestimation of $\Delta p_{t,1\text{-}2}$ with an AAPD of 32% and 16%, respectively. The results for RLZ-I under-estimated the measurements with an AAPD of 14%.

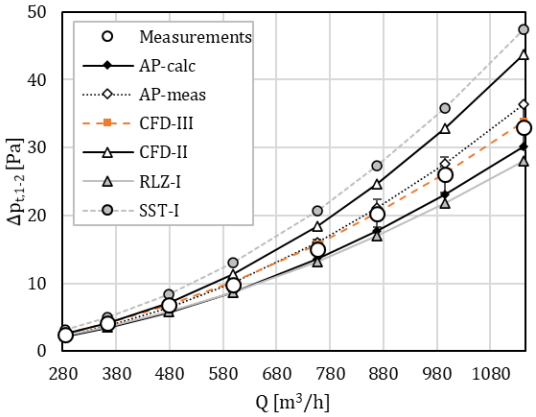

Fig. 6 - Pressure drop $\Delta pt_{,1\text{-}2}$ for configuration A.

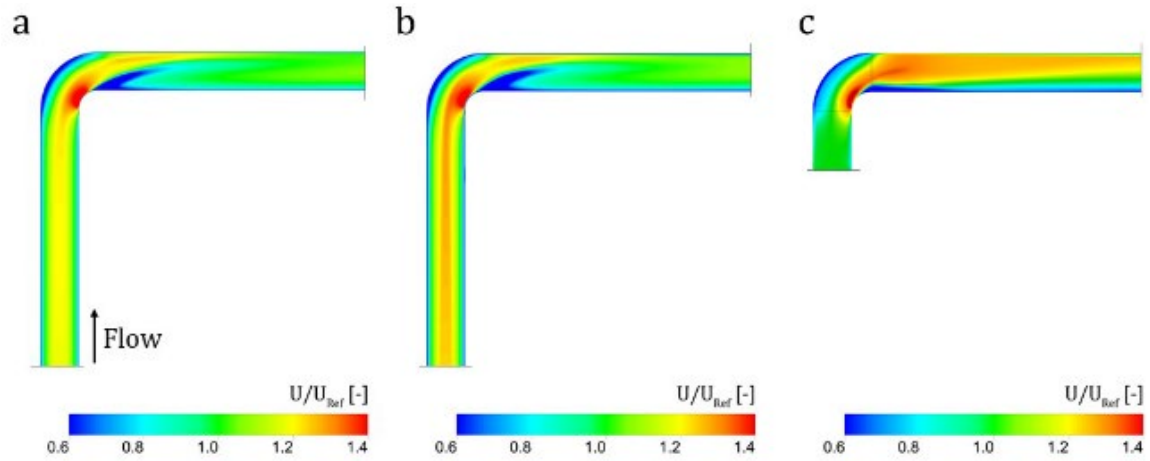

Fig. 7 - Contours of mean velocity ratio U/U_{Ref} for (a) RLZ-I, (b) CFD-II and (c) CFD-III, for configuration A.

Contours of mean velocity ratio are presented in Figure 7 for configuration A. The mean velocity ratio U/U_{Ref} is defined as the mean velocity magnitude U with respect to the inlet mean velocity U_{Ref} = 9 m/s. Differences between CFD methods RLZ-I (Fig. 7a) and CFD-II (Fig. 7b) were as follows. In general, larger regions of low velocity (blue color) were found in the close vicinity of the walls in the straight parts in the configuration for CFD-II (thicker boundary layer). For RLZ-I a larger gradient (thinner boundary layer) was observed near the wall in Fig 7a, while a higher mean velocity ratio was present in the center of the duct for CFD-II (see Fig. 7b) upstream of the elbow. A larger wake region in the region downstream of the elbow was observed for CFD-II. Compared to the CFD-I and CFD-II, a very dissimilar flow field was found for the CFD-III method (Fig. 7c). The size of the wake region downstream of the elbow was very small. Further downstream a large velocity gradient was observed over the complete cross-section of the duct.

5.3 Configuration B: Double elbow

The pressure drop results concerning configuration B are presented in Figure 8. While CFD-III showed a very good agreement with the measurement results for configuration A, for configuration B $\Delta p_{t,1\text{-}2}$ was overestimated with an AAPD of 64%. The pressure drop $\Delta p_{t,1\text{-}2}$ was also mostly overestimated by SST-I (AAPD = 46%), CFD-II (AAPD = 35%), AP-meas (AAPD = 31%) and AP-calc (AAPD = 19%). The best agreement was obtained by RLZ-I with an AAPD of 12%.

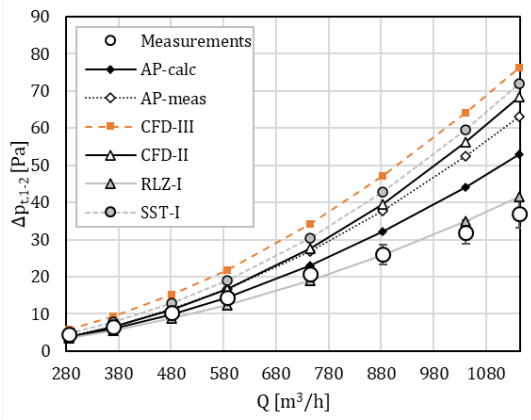

Fig. 8 - Pressure drop $\Delta pt_{,1\text{-}2}$ for configuration B.

For configuration B the contours of mean velocity ratio are given in Figure 9. Comparable flow characteristics were identified as those found for configuration A. Again a higher mean velocity ratio was observed in the center of the duct upstream of the elbows for CFD-II. In addition, the wake regions downstream of both corners were larger compared to those found for RLZ-I. This was most pronounced for the wake region near the downstream elbow. Also similar flow characteristics were observed for the CFD-III method. No recirculation areas in the wake regions downstream of the elbows could be identified and large regions of high mean velocity ratio were present. Downstream of the elbows, it took longer for the flow to stabilize while using the CFD-III method compared to the RLZ-I and CFD-II methods.

6. Discussion

For the single elbow configuration there was a fair agreement between the measured and analytically predicted pressure drops. With AAPDs of 7% and 13% for respectively AP-meas and AP-calc the agreement could be acceptable. However, as the system got more complex and another elbow was added, these AAPDs increased to 31% (AP-meas) and 19% (AP-calc). This large increase in error, especially for AP-meas as it directly used input values based on the onsite measurements, implicates that the flow field in a complex system might be too complex to accurately predict the pressure drop using analytical equations. However, the agreement with the investigated CFD methods was not much better in general. The CFD-III method showed a very good agreement in terms of pressure drop for the single elbow configuration. However, the deviating flow field raised concerns about whether this agreement was largely based on coincidence. These concerns were justified, as the prediction of the pressure drop for the double elbow configuration yielded an AAPD of 64%. Important flow features, like recirculation zones, wake regions and diffusion were not accurately modeled in the presented simulations. As the software only allowed pressure drop calculations over the complete domain, just the part between P1 and P2 was modeled. Therefore, the flow was not completely developed at P1. This could have impacted the results.

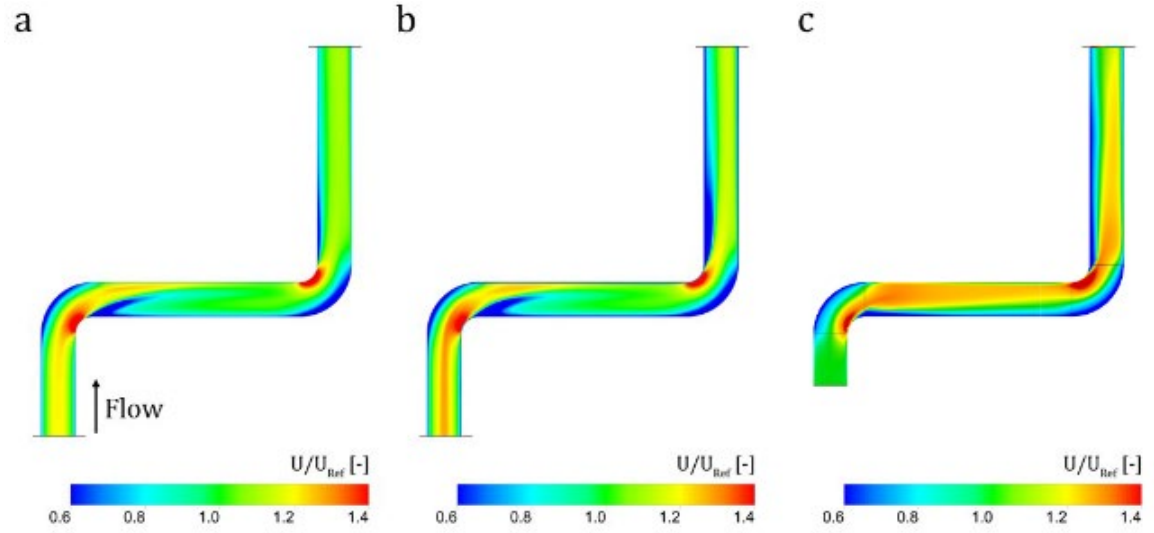

Fig. 9 - Contours of mean velocity ratio U/U_{Ref} for (a) RLZ-I, (b) CFD-II and (c) CFD-III, for configuration B.

For both configurations the CFD-II method overpredicted the pressure drop. A reason for this could be the fact that the k-ε turbulence model, together with wall functions, could overestimate the speed and size of the recirculation areas after flow separation [26, 27]. Wall functions are not capable of accurately predicting the separation point [28]. Overestimation of the wake and recirculation areas contributes to an increase in pressure drop. The CFD-II method used the k-ε turbulence model together with wall functions, while the RLZ-I used the same turbulence model but resolved the flow down to the viscous sublayer at the wall. This would theoretically lead to a better prediction of flow separation and wake regions. However, this method was not capable of modeling the roughness at the wall. This led to a larger velocity gradient near the wall. The decrease in velocity was smaller with no roughness, which partly explains the under-estimation of the pressure drop for using RLZ-I. The other CFD-I method, SST-I, is capable of taking wall roughness into account. However, for both configurations this method overpredicted the pressure drop. In accordance with existing literature on this topic [9] the modeling of roughness had a large impact on the pressure drop prediction. In the remainder of the larger ongoing research project, the use of lower k_S values will be studied as well.

In the current paper only several analytical and CFD methods were included. A general method to predict the pressure drop with satisfying accuracy was not yet found. This paper is part of a larger study in which the performance of additional methods will be assessed as well. At this moment only the use of coarse grids and the use of voxel-based CFD was investigated. As a wide range of simple/fast numerical methods is currently available, the use and performance of more methods will be considered. The aim is to find a fast and user-friendly tool with sufficient accuracy which can be used by engineers without the need for much knowledge on CFD. For benchmark purposes, also the performance of more sophisticated methods, like large eddy simulation or hybrid methods, will be assessed. In addition, measurements on additional complex duct configurations, to be used for validation purposes, is the subject of future work.

7. Conclusion

In this study the application of several CFD and analytical methods on the prediction of the pressure drop in the ventilation system design process was assessed. These included the performance of high-quality CFD on high-resolution grids, the use of simplified CFD by means of coarse-grid CFD and voxel-based CFD, and the use of analytical equations with loss coefficients from either existing literature or self-conducted measurements. Measurements on two duct configurations were performed and were used for validation purposes.

The hypothesis that the analytical prediction starts to deviate from the onsite situation as the system gets more complex holds for the investigated configuration and methods. However, also a satisfying CFD method was not yet found. For the CFD methods that allowed the modeling of roughness at the duct inner surface, the prediction of the pressure drop was highly sensitive to the applied roughness parameters. Though the applied roughness parameters were chosen based on a fitting process with experimental data for a straight duct, these parameters led to overprediction of the pressure drop for the investigated elbow configurations. For the high-resolution CFD method which could not include surface roughness at the walls, the calculated pressure drop was much lower. While the investigated voxel-based CFD method showed an absolute average percentage difference of only 3% with the measurements for the single elbow configuration, it greatly overestimated the measured pressure drop by 64% on average. Based on the investigated methods and configurations in this study, no general sufficiently accurate method for predicting the pressure drop could yet be chosen.

Acknowledgements

This work has been supported by the Flemish Agency for Innovation and Entrepreneurship (VLAIO) in the Flux50 project Smart Ventilation (HBC.2020.2520).

References

[1] Tsal R.J., Behls H.F., Mangel R. T-method duct design – Part 1: optimisation theory and Part 2: calculation procedure and economic analysis. ASHRAE Trans. 1988;94(2): 90–151.

[2] Jorens S., Sörensen K., Verhaert I., de Corte A. Air distribution system design optimisation in non-residential buildings: Problem formulation and generation of test networks. J. Build. Eng. 2017;12: 60-67.

[3] Fischer D. Ventilation duct design by CFD-technology. Proc of Automotive Sim 1991: 169-180.

[4] Smith S.J. Determination of k-factors of HVAC system components using measurement and CFD modelling. PhD thesis, University of Nottingham. 1998.

[5] Beach R., Prahl D. Computational fluid dynamics analysis of flexible duct junction box design. US Department of Energy. 2013.

[6] Mumma S., Mahank T., Ke Y. Close coupled ductwork fitting pressure drop. HVAC&R Res. 1997;3(2): 158-177.

[7] Mumma S., Mahank T., Ke Y. Analytical determination of duct fitting loss-coefficients. Appl. Energy 1998;61: 229-247.

[8] Moujaes S.F., Deshmukh S. Three-Dimensional CFD Predications and Experimental Comparison of Pressure Drop of some Common Pipe Fittings in Turbulent Flow, J. Energy Eng. 2006;132(2): 61-66.

[9] Liu W., Long Z., Chen Q. A procedure for predicting pressure loss coefficients of duct fittings using CFD (RP-1493) HVAC&R Res. 2012;18(6): 1168–1181.

[10] Manning A., Wilson J., Hanlon N., Mikjaniec T. Prediction of duct fitting losses using computational fluid dynamics. HVAC&R Res. 2013;19(4): 400-411.

[11] Liu W., Jin M., Chen C., You R., Chen Q.. Implementation of a fast fluid dynamics model in OpenFOAM for simulating indoor airflow. Numer. Heat. Tr. A-App. 2016;69(7): 748-762.

[12] Khan M.A.I., Delbosc N., Noakes C., Summers J. Real-time flow simulation of indoor environments using lattice Boltzmann method. Build. Simul. 2015;8: 405-414.

[13] Wang H., Zhai J. Application of coarse-grid computational fluid dynamics on indoor environment modeling: optimising the trade-off between grid resolution and simulation accuracy, HVAC&R Res. 2012;18(5): 915-933.

[14] Chen Q., Xu W. A zero-equation turbulence model for indoor airflow simulation, Energy Build. 1998;28(2): 137-144.

[15] ANSYS Inc. ANSYS Discovery Live 2020 R1 User's Guide. 2020.

[16] ANSI/ASHRAE Standard 120-2017. Method of Testing to Determine Flow Resistance of HVAC Ducts and Fittings. 2017. Atlanta, GA: ASHRAE

[17] Testo data sheet, Testo 480 Multi-function VAC measuring instrument. https://static-int.testo.com/media/ff/0a/bbcc0227c912/testo-480-Data-sheet.pdf

[18] ASHRAE Handbook – Fundamentals (SI). 2001. Atlanta. GA: ASHRAE. Chapter 14 – Measurements and instruments.

[19] ASHRAE Handbook – Fundamentals (SI). 2005. Atlanta. GA: ASHRAE. Chapter 35 – Duct Design.

[20] Idelchik I.E., Steinberg M.O., Malyavskaya G.R., Martynenko O.G. 1994. Handbook of hydraulic resistance. 3rd ed. CRC Press/Begell House. Boca Raton. Ann Arbor. London. Tokyo.

[21] Shih T.H., Liou W.W., Shabbir A., Zhu J. A new k-ε eddy-viscosity model for high Reynolds number turbulent flows - model development and validation. Comput. Fluids. 1995;24(3): pp. 227-238.

[22] Menter F. Eddy viscosity transport equations and their relation to the k-ε model. J. Fluids Eng. 1997;119: 876-884

[23] van Hooff T., Blocken B. Coupled urban wind flow and indoor natural ventilation modeling on a high-resolution grid: a case study for the Amsterdam ArenA stadium. Environ. Model. Softw. 2010;25: 51-65

[24] ANSYS Inc, ANSYS FLUENT 2021 R1 User's Guide. 2021.

[25] Ye, T., Mittal, R., Udaykumar, H.S. and Shyy, W., An accurate Cartesian grid method for viscous incompressible flows with complex immersed boundaries. J. Comput. Phys.. 1999;156(2): 209-240.

[26] Murakami S. Comparison of various turbulence models applied to a bluff body. J. Wind Eng. Ind. Aerodyn. 1993;46: 21-36

[27] Tominaga Y., Mochida A., Murakami S., Sawaki S. Comparison of various revised k–ε models and LES applied to flow around a high-rise building model with 1:1:2 shape placed within the surface boundary layer. J. Wind Eng. Ind. Aerodyn. 2008;96(4): 389-411

[28] Menter F.R. Improved two-equation k-turbulence models for aerodynamic flows. NASA technical memorandum. 1992(1) 103975.